Perovskite Solar Cells with Enhanced Fill Factors using Polymer-Capped Solvent Annealing

Jaemin Kong,[†‡] Hanyu Wang,[‡] Jason A. Röhr,[†] Zachary S. Fishman,[‡] Yuanyuan Zhou,[#] Mingxing Li,[§] Mircea Cotlet,[§] Geunjin Kim,[‖] Christopher Karpovich,[‡] Francisco Antonio,[‡] Nitin P. Padture,[#] and André D. Taylor*[†‡]

[†]Department of Chemical and Biomolecular Engineering, New York University Tandon School of Engineering, Brooklyn, NY 11201, USA
E-mail: andre.taylor@nyu.edu

[‡]Department of Chemical and Environmental Engineering, Yale University, New Haven, CT 06511, USA

[#]School of Engineering, Brown University, Providence, Rhode Island 02912, USA

[§]Center for Functional Nanomaterials, Brookhaven National Laboratory, Upton, New York 11973, USA

[‖]Division of Advanced Materials, Korea Research Institute of Chemical Technology (KRICT), Daejeon 34114, South Korea

Keywords: perovskite solar cells, large clusters, polymer-capped solvent annealing, hot air blower, high fill factor

Abstract

Despite huge improvements in power conversion efficiencies of perovskite solar cells, the technology is still limited by fill factors at around 80%. Here, we report perovskite solar cells having exceptionally high fill factors of 85% and enhanced open-circuit voltage without sacrificing short-circuit current through a polymer-capped solvent annealing process assisted by a hot air blower. During the solvent annealing process with a hot air blower, the perovskite surface flattens, and the perovskite grains agglomerate together into micrometer-sized clusters having enlarged α-phase crystallites while the δ-phase simultaneously disappears. The optimized structure reduces energetic disorder and trap-assisted recombination in the perovskite layer, resulting in an enhanced efficiency from 18.2% to 19.8% in average and improved device lifetime. Our results provide a pathway to increase the device efficiency and stability of perovskite solar cells and have the potential to stimulate research on scalable single-crystal perovskite layer fabrication in optoelectronic devices.

Organic-inorganic metal halide perovskite solar cells have received great attention due to their excellent optoelectronic properties including a large absorption coefficient (~10^5 cm^{-1}),[1] a low exciton binding energy (~20 meV),[2] a relatively long charge-carrier diffusion length (~1 μm),[3] and have shown dramatic improvements in the power conversion efficiency (PCE) from 3.8% to a certified 25.2% over the past few years.[4] Based on the Shockley–Queisser limit, a theoretical PCE limit for E_g of ~1.6 eV is approximately 30% with a short circuit current density (J_{SC}) of ~25 mA cm^{-2}, open circuit voltage (V_{OC}) of ~1.3 V and fill factor (FF) of ~90%.[5-7] With record cells having a J_{SC} of ca. 24 mA cm^{-2}, a V_{OC} of 1.10~1.16 V and a FF of 73~81%,[8-10] there is still room for PCE improvement if the parameters such as V_{OC} and FF could be further enhanced.

A feasible way to further enhance the solar cell parameters is to reduce defects in the solar cells.[11-12] In a polycrystalline perovskite layer, defects and/or halide segregations, which could act as trap/recombination centers, are typically concentrated at grain boundaries and interfaces.[13] Bi *et al.* achieved an enhanced V_{OC} of 1.16 V with a high J_{SC} of 24.6 mA cm^{-2} by adding an excess of lead iodide (PbI_2) which induced the growth of bigger perovskite grains/crystallites.[8] Enlarging the crystallite size and reducing the area of grain boundaries lowered the trap density of the perovskite layer, giving rise to a higher V_{OC}; however, the FF of the solar cell still exhibited a relatively low value of 73%. Although the excessive PbI_2 can be used as seeds to grow bigger perovskite crystallites, the excess of PbI_2 might give rise to additional defects such as non-stoichiometric lattice disorder in the grains or halide segregation at the grain boundaries. Recently, Yang *et al.* reported an internal passivation method to reduce compositional point defects (*i.e.*, I-deficient intermediates) that are charge-balanced by positive ions in the perovskite layer. By introducing additional triiodide ions, deep-level traps were significantly reduced while the proportion of α-$FAPbI_3$ phases in the resulting layer increased, which led to an enhanced FF of 81.9%.[9] Although the deep-level traps were removed with the

aid of additional triiodide ions, V_{OC} was still limited at ~1.1 V. This may originate from another defect source; for example, iodine interstitials or iodine enrichment at grain boundaries, resulting in a reduced band gap.[14]

Another strategy to reduce defects in the perovskite solar cells has been sought by employing polymers or small molecules in the anti-solvents during a perovskite film fabrication process.[15-18] By dripping polymer (or small molecule) solutions, instead of pure organic solvents, inner passivation layers have been formed in between perovskite and hole transporting layers, which could reduce interfacial defects. Moreover, the thin organic layers could act as templates for nucleation and crystal growth of perovskite layers. However, the previous works have been done with diluted solutions such as below 10 mg mL^{-1} since the polymer layers were also intended to be used as inner passivation layers; if the organic layers are too thick, regardless of their band gaps and energy levels, they turned to be another defect sites by hampering charge transport and collection.[19] For that reason, the impact of high concentration of organic solutions, i.e., thicker organic films, to perovskite layer formations has been overlooked so far.

Here, we demonstrate that high concentration of polystyrene solution could lead to larger clustered grains with the size of a few micrometers in the perovskite layer, resulting in exceptionally high FF of 85% and V_{OC} of ~1.15V (without sacrificing J_{SC}), simultaneously. A hot air blower enables the thick top polymer film to be dried prior to the underlying still-wet perovskite layer, giving a time for perovskite grains to grow along with the flat dried polymer film. Moreover, the dried polymer film retards the solvent vaporization of the semi-dried perovskite layer in order for preformed perovskite gains to agglomerate together to form larger clusters. Furthermore, we found that this process also reduces the occurrence of δ-phase, which helps minimize structural defects in the perovskite layer. A simple rinsing step using a common organic solvent clearly removes the polystyrene polymer film after the beneficial process, which makes sure that the insulating polystyrene film should not adversely affect the charge

transport and collection, so that the resulting perovskite layer could possess reduced energetic disorder and less trap-assisted recombination which consequently lead to enhanced efficiencies and improved stabilities. Last but not least, we noted that the significantly reduced surface roughness could provide a great platform for a large area solar cell manufacturing.

Fig. 1a depicts a schematic of the polymer-capped solvent annealing process and top-view SEM images of the perovskite layers processed with pure CB and CB containing 1, 2, 3, 5 wt% polystyrene (PS), respectively. We found that 5 wt% is the highest polystyrene concentration we could employ before we started to experience drying issues where the PS films would tear during the hot air drying process. Although DMF and DMSO, which are the solvents for perovskite precursors, can permeate through the polystyrene films, we believe that thick polystyrene films will not allow for a rapid evaporation of DMF and DMSO during the drying process. During conventional processing of perovskite layers, pure chlorobenzene (CB) solvent is dripped during the spin coating process of the perovskite solution on a TiO_2-Cl/ITO/glass substrate,[20-21] and the resultant film is shown in the SEM image (Fig. 1b). However, during the polymer-capped solvent-annealing process, a PS solution is dripped while the perovskite solution coated substrate is spinning. During this polymer-coating process, a semi-dried PS film is formed onto a wet perovskite layer, which confines the perovskite solvents (DMF and DMSO) in between the PS film and the bottom substrate since the PS film is almost neither soluble in DMF nor DMSO. After forming a thin layer of PS film on the wet perovskite layer, the substrate is kept in a N_2 glove box at room temperature for 5 min. This method is akin to a conventional solvent annealing process which has been widely used for organic solar cells to provide time to induce self-alignment of the organic molecules and to form higher crystallinities of the photoactive layer.[22-23] After the PS-capped solvent annealing process, the samples were placed under a hot air blower to dry the PS film first from the top side. This drying process renders the underlying wet perovskite layer flat. If this heat gun step is skipped, it is observed that the

perovskite layer surface becomes bumpy and rough (Fig. S1a); for example, in the case of the 5% PS solution treatment directly followed by a hot plate annealing, the root mean square (RMS) roughness of the perovskite layer is as high as 64 nm, and the maximum roughness depth (R_{max}) reaches 494 nm which is almost same length scale as the film thickness. Since both the PS and the perovskite layers are wet right after the polymer-coating process, it is reasonable to assume that the PS film will dry prior to the perovskite layer. The wet perovskite layer will for that reason dry along with the flat dried PS film surface. We also believe that the PS films will stiffen and flatten at a PS concentration of 3% or higher. In fact, we observe an increase roughness of the perovskite surface when low concentrations (0% to 2%) of PS is employed (Fig. S1b-d). Beyond a PS concentration of 3%, the surface starts to flatten (Fig. S1e,f). After drying the top PS film with a heat gun blower for 5 min, the substrate is moved onto a hot plate to completely dry all layers, including the perovskite layer. After the whole drying processes are completed, the top PS layer is removed by washing off the substrate with CB. Using polarization modulation-infrared reflection absorption spectroscopy (PM-IRRAS), which has advantage of high surface sensitivity, it was verified that no detectable PS remains on the perovskite film after washing (Fig. S2). SEM images of the resultant perovskite films are shown in Fig. 1c-f. Noticeably, beyond a 2% PS solution treatment (Fig. 1d), the grains start clustering and the grain sizes increase up to 1~2 μm which is almost an order of magnitude larger than that of the control sample (Fig. 1b). Moreover, the RMS roughness is significantly reduced from 17.7 to 10.1 nm, and the R_{max} also decreases from 138 to 85 nm when comparing a pure CB treated to the 5% PS solution treated perovskite film morphologies (Fig. S1b-f).

To develop a deeper understanding of the changes in the microstructure resulting from the polymer-capped solvent-annealing processes, we studied XRD patterns of the treated perovskite layers (Fig. 2a). From the XRD pattern for the control sample (pure CB), we observe a peak ($2\theta \approx 11.5°$) for photo-inactive δ-$FAPbI_3$ phase (i.e., yellow phase).[24-25] However, as the

PS concentration increases, the δ-phase peak reduces, and finally disappears after 2% PS solution (Fig. 2b). Converting from α to δ phase is energetically spontaneous, and favorably occurs at the grain boundaries.[26-27] Since we brought the samples out of N_2-glove box for XRD measurement, the δ phase might occur during the XRD measurement in air. Less grain boundaries in the high concentrated PS-treated samples may reduce the probability of δ phase occurance in air. On the contrary, δ-to-α phase transformation needs energy; for example, a thermal energy by a hot plate.[28] Liu *et al*. recently reported that a large grain size in δ phase intermediate films is essential for the growth of high-quality α phase perovskite films.[28] Thus, the preformed large grains/clusters during the polymer-capped solvent annealing process could favorably promote a growth of high-quality α-phase perovskite layer. Indeed, we note that the photoactive α-phase peak centered at $2\theta \approx 14°$ significantly intensifies and the full width half maximum (FWHM) of the peak reduces dramatically, which reflects that the α-phase crystallites substantially grow from 50 nm to 90 nm as the PS solution concentration increases.[25]

To investigate the impact of the polymer-capped solvent annealing on the device performance, we fabricated solar cells using pure CB solvent and PS solutions with different concentrations (Fig. 3a). Using up to 2% PS the V_{OC} slightly decreases, but above 2% PS the V_{OC} increases and reaches a maximum value of 1.16 V at 5% PS (Fig. 3b). The slight V_{OC} reduction from 1.128 V to 1.125 V might be attributed to the rough surface morphology of the perovskite layer (Fig. S1d). The RMS and R_{max} increase from 17.7 nm to 30.5 nm and from 138 nm to 196 nm, respectively, when the PS concentration is increased from 0% to 2%. The rougher surface of the perovskite layer might cause an uneven thickness of the Spiro-OMeTAD hole transporting layer on the rough perovskite layer surface. Since the R_{max} of the perovskite layer processed with 2% PS solution is 196 nm, the thickness of the Spiro-OMeTAD coated onto the ridges of perovskite layer can be lower than that coated onto the flatter surface of the perovskite layer (Fig. S3). This agrees with a recent report by Kim *et al.* who reported that when the

thickness of the Spiro-OMeTAD is below 180 nm, the V_{OC} of the solar cells shows a declining trend, while thicker Spiro-OMeTAD layer provides more reproducible performance.[29] In the paper and elsewhere, however, the detailed mechanism on the correlation between thickness of Spiro-OMeTAD and V_{OC} has not been elaborated. For a further understanding, in-depth studies need to be done in the future. As for the values for the FFs, a remarkable increase (FF≈85%) was found employing the 3% PS solution with a narrower distribution of the FF (Fig. 3c). Taken together, the polymer-capped solvent-annealing process enhanced the average PCE from 18.2% to 19.8%, with the PCE of the best device found to be 21% when 3% PS was used (Fig. 3d, Fig. S4 and S5, and Table S1). However, this approach might not be able to remove hysteresis issues in current density-voltage (*J-V*) characteristics although the fill factor in a reverse-to-forward bias sweep was enhanced compared to the one from the control device (Fig. S6, Table S1). Nevertheless, PS-treated solar cell shows a reduced chemical capacitance (Fig. S7) which implies that capacitive hysteresis should be reduced accordingly. Considering the experimental result, the limitation of FF enhancement in a reverse-to-forward bias sweep might be attributed to other source such as a non-capacitive hysteresis which could occur due to an interfacial modification and/or a contact reactivity caused by perovskite ionic motions and/or halide vacancies. Thus, this type of hysteresis should be dealt with different approaches such as alkali metal cation (e.g., K^+) addition in the bulk and/or alkali metal cation treatment on an electron transport layer (ETL),[30-32] which is beyond our current scope. Therefore, a follow-up study using a potassium treatment together with our polymer-capped solvent annealing or changing the device structure to the p-i-n architecture might be needed to see if both the energetic disorder and the halide vacancies could be controlled at once in the near future.

To elucidate the impact of the polymer-capped solvent-annealing process on the solar cell parameters, we further analyzed the solar cell processed with 3% PS solution which exhibited the highest values for the PCE and FF. We compare photoluminescence (PL) data which shows

a peak shift to shorter wavelength (762 nm to 758 nm) and narrower FWHM (46 nm to 44.7 nm) upon the PS-capped solvent annealing process (Fig. 4a and Fig. S8a). Tauc plots also show shifts in absorption onsets to higher energies (1.579 eV to 1.583 eV) along with sharper slopes (Fig. S8b). These results may imply that the smeared-out band edge recedes from the band gap to some extent, which could be due to reduction in energetic disorder in the solar cells.[33] To support this postulation we characterized the energetic disorder in the solar cells by measuring the distribution of the electronic density of states (DOS). To do this, we extracted chemical capacitance (C_μ) using a widely used equivalent circuit for planar heterojunction perovskite solar cells (Fig. S7a).[34-38] The C_μ at open-circuit condition, under different light intensities, reflect the density of occupied charge carriers at each quasi-Fermi level in the solar cells. This method can therefore be used to record the variation in the DOS near the band edges. We fit the DOS with either Gaussian or Urbach tail (Fig. 4b)[37-39] Detailed descriptions for both can be found in the experimental section and SI (Fig. S7b). From the Gaussian fit, the width of distribution (or degree of energetic disorder) is found to decrease from 121 meV to 62 meV upon the polymer-capped solvent annealing with 3% PS. From the Urbach tail fitting, the characteristic energy decreased from 71 eV to 44 eV. Since both characteristic figures could represent the distributions of gap states near the band edges, the reduction in either energy could reflect the recession of smeared-out band edge, which is a likely cause for the observed V_{OC} enhancement.

The less disordered perovskite layer seems to have less trap-induced recombination. Fig. 4c shows the V_{OC} variation as a function of the light intensity, which is an indicator for the degree of trap assisted recombination in the device.[40] If the slope of the plot is closer to 2, there is a dominant trap-assisted recombination in the solar cells.[41] On the other hand, when it is less than 2, it infers that trap-assisted recombination is suppressed.[11] In Fig. 4c, the 3% PS treated perovskite solar cell shows a lower slope (1.19 $k_BT\ q^{-1}$) than that of pure CB treated perovskite solar cell (1.41 $k_BT\ q^{-1}$). Hence, it could be expected that the polymer-capped solvent-annealing

process suppresses trap-assisted recombination. Furthermore, the fill factor is mainly affected by carrier recombination. Therefore, the polymer-capped solvent-annealing process might reduce the energetic disorder as well as trap-assisted recombination in the solar cell, resulting in a high V_{OC} and FF.

When we plot the FF as a function of the V_{OC}, a significant improvement in ideality factor is observed upon the polymer-capped solvent-annealing process. By adopting an equation from traditional inorganic p-n junction solar cells,[42-43] we can express FF as

$$\mathrm{FF} = \frac{\tilde{v}_{oc} - \ln(\tilde{v}_{oc} + 0.72)}{\tilde{v}_{oc} + 1} \quad (1)$$

where $\tilde{v}_{oc}$ is the V_{OC} normalized to the thermal voltage,

$$\tilde{v}_{oc} = \frac{V_{OC}}{n_{id} kT/q} \quad (2)$$

k is the Boltzmann constant, T is temperature, q is the elementary charge, and n_{id} is an ideality factor which is related to a characteristic diode behavior; as n_{id} is approaching unity, the diode becomes ideally operating.[44] In Fig. 4d, it is found that a crossing point of the V_{OC} and FF for the control solar cell is lying between n_{id} = 2.0 and 2.5 whereas for the polymer-capped solvent-annealed solar cell is located at n_{id} = 1.5. Therefore, the polymer-capped solvent-annealing process might facilitate a better solar cell operation by reducing disorder and recombination in the solar cells.

To investigate the stability of the perovskite films, without any direct influence of the back co ntacts, we prepared two batches of films: One batch with films treated with pure CB and the o ther batch with films treated with the 3% PS solution. Each batch contained five sets of films, each containing 3 cells (30 cells in total), that were designed to be exposed to air (RH ≈ 20%, T ≈ 80 °C) for 0, 1, 5, 10, 20 days, respectively. Before exposing the perovskite films to air, al l the PS-treated perovskite films were washed with CB to remove the entirety of the PS, and w

ere subsequently dried with N_2. As LiTFSI, which is normally used as a dopant to the Spiro-O MeTAD hole-transport layer, can negatively affect device stability, we performed the aging pr ocess before completing the full solar cell architecture, i.e., before processing the hole-transpo rt layer and Au electrode. After certain periods of exposure time, the Spiro-OMeTAD and Au electrode were deposited on the aged perovskite films, and completely fabricated solar cells were tested. As shown in Fig. 5a, the PCEs for the control films treated with CB drop by more than 20% after 20-day air exposure whereas the PCEs for the PS-capped solvent annealed films decreased by less than 10% during the same period of time (Fig. 5a). Notably, the efficiency difference between the two groups is significantly widened from 5% to more than 20% after 20 days of air exposure. The slow reduction in PCE for the PS-capped solvent-annealed samples might be attributed to the reduced reactive area of the grain boundaries and the enhanced crystallite sizes.[45-46] Moreover, the PS-capped solvent annealing process might be beneficial for the large area solar cell fabrication since this technique renders the surface of the perovskite layer flatter (Fig. S1). In large area solar cells and modules, a single pinhole may cause the entire cell to shunt, which dramatically reduces the device performance or could even lead to device failure.[47] In our large area solar cells with the active area = 1 cm^2 the PCEs from the PS-treated solar cells are higher than those of the control cells treated with CB, further exhibiting a narrower PCE deviation (Fig. 5b and Table S2). The smooth and flat perovskite films (Fig. S1) may also facilitate better contact with the Spiro-OMeTAD layer, preventing pinholes and physical defects at the interface.[47-48]

In summary, we demonstrate that a polymer-capped solvent-annealing process assisted by a hot air blower suppresses the occurrence of δ-phase perovskites and simultaneously increases the crystallite size of α-phase perovskites, possibly leading to less trap-assisted recombination and lower energetic disorder of the solar cells. Thus the polymer-capped solvent-annealed solar cells exhibit FFs as high as 85% with an enhanced V_{OC} of up to 1.15V without sacrificing any

J_{SC}. In addition, the compactly packed clusters of the perovskite grains reduce the degree of degradation, making the solar cells stable in air over a duration of 20 days. Moreover, the flat perovskite layer surface which was induced by the PS film is beneficial for the large-area solar cell fabrication with high reliability. Our approach and results show great potential for further efficiency improvements, and could be widely used to control the grain/crystallite size of polycrystalline perovskite layer for optoelectronic devices.

ASSOCIATED CONTENT

Supporting Information

The Supporting Information is available free of charge on the ACS Publications website at DOI: xxx.

>> Experimental methods, AFM topology images, Polarization Modulation-Infrared Reflection Absorption Spectroscopy, Cross-sectional SEM images, EQE, Time-dependent power density at the voltage of maximum power output, Equivalent circuit of IS response and chemical capacitance plot , Photoluminescence and Tauc plot and tables (PDF)

AUTHOR INFORMATION

Corresponding Authors

*E-mail: andre.taylor@nyu.edu

Notes

The authors declare no competing financial interest.

Acknowledgements

The authors gratefully acknowledge the National Science Foundation NSF-PECASE award (CBET-0954985) and New York University for partial support of this work. The Yale Institute for Nanoscience and Quantum Engineering (YINQE) and NSF MRSEC DMR 1119826 (CRISP) provided facility support. The research at Brown University was performed under the

funding support from the National Science Foundation (OIA-1538893 and OIA-1929019) and Office for Naval Research (N00014-17-1-2232). The research used resources of the Center for Functional Nanomaterials, which is a U.S. DOE Office of Science Facility, at Brookhaven National Laboratory under Contract No. DE-SC0012704. We thank Jacob A. Spies for fruitful discussions.

References

(1) Kojima, A.; Teshima, K.; Shirai, Y.; Miyasaka, T. Organometal halide perovskites as visible-light sensitizers for photovoltaic cells. *J Am Chem Soc* **2009,** *131* (17), 6050-1, DOI: 10.1021/ja809598r.
(2) Yang, Z.; Surrente, A.; Galkowski, K.; Bruyant, N.; Maude, D. K.; Haghighirad, A. A.; Snaith, H. J.; Plochocka, P.; Nicholas, R. J. Unraveling the Exciton Binding Energy and the Dielectric Constant in Single-Crystal Methylammonium Lead Triiodide Perovskite. *J Phys Chem Lett* **2017,** *8* (8), 1851-1855, DOI: 10.1021/acs.jpclett.7b00524.
(3) Stranks, S. D.; Eperon, G. E.; Grancini, G.; Menelaou, C.; Alcocer, M. J. P.; Leijtens, T.; Herz, L. M.; Petrozza, A.; Snaith, H. J. Electron-Hole Diffusion Lengths Exceeding 1 Micrometer in an Organometal Trihalide Perovskite Absorber. *Science* **2013,** *342* (6156), 341-344, DOI: 10.1126/science.1243982.
(4) NREL Best Research Cell Efficiencies. https://www.nrel.gov/pv/cell-efficiency.html (accessed September 10, 2019).
(5) Shockley, W.; Queisser, H. J. Detailed Balance Limit of Efficiency of P-N Junction Solar Cells. *J Appl Phys* **1961,** *32* (3), 510-&, DOI: Doi 10.1063/1.1736034.
(6) Sha, W. E. I.; Ren, X. G.; Chen, L. Z.; Choy, W. C. H. The efficiency limit of CH3NH3PbI3 perovskite solar cells. *Appl Phys Lett* **2015,** *106* (22), DOI: Artn 221104

10.1063/1.4922150.
(7) Ruhle, S. Tabulated values of the Shockley-Queisser limit for single junction solar cells. *Sol Energy* **2016,** *130*, 139-147, DOI: 10.1016/j.solener.2016.02.015.
(8) Bi, D. Q.; Tress, W.; Dar, M. I.; Gao, P.; Luo, J. S.; Renevier, C.; Schenk, K.; Abate, A.; Giordano, F.; Baena, J. P. C.; Decoppet, J. D.; Zakeeruddin, S. M.; Nazeeruddin, M. K.; Gratzel, M.; Hagfeldt, A. Efficient luminescent solar cells based on tailored mixed-cation perovskites. *Sci Adv* **2016,** *2* (1), DOI: UNSP e1501170

10.1126/sciadv.1501170.
(9) Yang, W. S.; Park, B. W.; Jung, E. H.; Jeon, N. J.; Kim, Y. C.; Lee, D. U.; Shin, S. S.; Seo, J.; Kim, E. K.; Noh, J. H.; Seok, S. I. Iodide management in formamidinium-lead-halide-based perovskite layers for efficient solar cells. *Science* **2017,** *356* (6345), 1376-+, DOI: 10.1126/science.aan2301.
(10) Jung, E. H.; Jeon, N. J.; Park, E. Y.; Moon, C. S.; Shin, T. J.; Yang, T. Y.; Noh, J. H.; Seo, J. Efficient, stable and scalable perovskite solar cells using poly(3-hexylthiophene). *Nature* **2019,** *567* (7749), 511-+, DOI: 10.1038/s41586-019-1036-3.
(11) Sherkar, T. S.; Momblona, C.; Gil-Escrig, L.; Avila, J.; Sessolo, M.; Bolink, H. J.; Koster, L. J. A. Recombination in Perovskite Solar Cells: Significance of Grain Boundaries, Interface Traps, and Defect Ions. *Acs Energy Lett* **2017,** *2* (5), 1214-1222, DOI: 10.1021/acsenergylett.7b00236.
(12) Wang, F.; Bai, S.; Tress, W.; Hagfeldt, A.; Gao, F. Defects engineering for high-performance perovskite solar cells. *npj Flexible Electronics* **2018,** *2* (1), 22, DOI: 10.1038/s41528-018-0035-z.
(13) Tang, X. F.; van den Berg, M.; Gu, E. N.; Horneber, A.; Matt, G. J.; Osvet, A.; Meixner, A. J.; Zhang, D.; Brabec, C. J. Local Observation of Phase Segregation in Mixed-Halide Perovskite. *Nano Lett* **2018,** *18* (3), 2172-2178.
(14) McKenna, K. P. Electronic Properties of {111} Twin Boundaries in a Mixed-Ion Lead Halide Perovskite Solar Absorber. *Acs Energy Lett* **2018,** *3* (11), 2663-2668.
(15) Bi, D. Q.; Yi, C. Y.; Luo, J. S.; Decoppet, J. D.; Zhang, F.; Zakeeruddin, S. M.; Li, X.; Hagfeldt, A.; Gratzel, M. Polymer-templated nucleation and crystal growth of perovskite films for solar cells with efficiency greater than 21%. *Nat Energy* **2016,** *1*.
(16) Zhang, F.; Shi, W. D.; Luo, J. S.; Pellet, N.; Yi, C. Y.; Li, X.; Zhao, X. M.; Dennis, T. J. S.; Li, X. G.; Wang, S. R.; Xiao, Y.; Zakeeruddin, S. M.; Bi, D. Q.; Gratzel, M. Isomer-Pure Bis-PCBM-Assisted Crystal Engineering of Perovskite Solar Cells Showing Excellent Efficiency and Stability. *Adv Mater* **2017,** *29* (17).
(17) Li, F. C.; Yuan, J. Y.; Ling, X. F.; Zhang, Y. N.; Yang, Y. G.; Cheung, S. H.; Ho, C. H. Y.; Gao, X. Y.; Ma, W. L. A Universal Strategy to Utilize Polymeric Semiconductors for Perovskite Solar Cells with Enhanced Efficiency and Longevity. *Adv Funct Mater* **2018,** *28* (15).
(18) Wu, Y. H.; Wang, P.; Wang, S. B.; Wang, Z. H.; Cai, B.; Zheng, X. J.; Chen, Y.; Yuan, N. Y.; Ding, J. N.; Zhang, W. H. Heterojunction Engineering for High Efficiency Cesium Formamidinium Double-Cation Lead Halide Perovskite Solar Cells. *Chemsuschem* **2018,** *11* (5), 837-842.
(19) Li, X.; Li, W.; Yang, Y.; Lai, X.; Su, Q.; Wu, D.; Li, G.; Wang, K.; Chen, S.; Sun, X. W.; Kyaw, A. K. K. Defects Passivation With Dithienobenzodithiophene-based π-conjugated Polymer for Enhanced Performance of Perovskite Solar Cells. *Solar RRL* **2019,** *3* (6), 1900029, DOI: 10.1002/solr.201900029.
(20) Zhang, H. Y.; Shi, J. J.; Zhu, L. F.; Luo, Y. H.; Li, D. M.; Wu, H. J.; Meng, Q. B. Polystyrene stabilized perovskite component, grain and microstructure for improved efficiency and stability of planar solar cells. *Nano Energy* **2018,**

43, 383-392, DOI: 10.1016/j.nanoen.2017.11.024.
(21) Li, M. H.; Yan, X. Q.; Kang, Z.; Huang, Y. H.; Li, Y.; Zhang, R. X.; Zhang, Y. Hydrophobic Polystyrene Passivation Layer for Simultaneously Improved Efficiency and Stability in Perovskite Solar Cells. *Acs Appl Mater Inter* **2018,** *10* (22), 18787-18795, DOI: 10.1021/acsami.8b04776.
(22) Huang, J. S.; Goh, T.; Li, X. K.; Sfeir, M. Y.; Bielinski, E. A.; Tomasulo, S.; Lee, M. L.; Hazari, N.; Taylor, A. D. Polymer bulk heterojunction solar cells employing Forster resonance energy transfer. *Nat Photonics* **2013,** *7* (6), 480-486, DOI: 10.1038/Nphoton.2013.82.
(23) Goh, T.; Huang, J. S.; Bartolome, B.; Sfeir, M. Y.; Vaisman, M.; Lee, M. L.; Taylor, A. D. Panchromatic polymer-polymer ternary solar cells enhanced by Forster resonance energy transfer and solvent vapor annealing. *J Mater Chem A* **2015,** *3* (36), 18611-18621, DOI: 10.1039/c5ta04905a.
(24) Binek, A.; Hanusch, F. C.; Docampo, P.; Bein, T. Stabilization of the Trigonal High-Temperature Phase of Formamidinium Lead Iodide. *J Phys Chem Lett* **2015,** *6* (7), 1249-1253, DOI: 10.1021/acs.jpclett.5b00380.
(25) Ono, L. K.; Juarez-Perez, E. J.; Qi, Y. B. Progress on Perovskite Materials and Solar Cells with Mixed Cations and Halide Anions. *Acs Appl Mater Inter* **2017,** *9* (36), 30197-30246, DOI: 10.1021/acsami.7b06001.
(26) Yun, J. S.; Kim, J.; Young, T.; Patterson, R. J.; Kim, D.; Seidel, J.; Lim, S.; Green, M. A.; Huang, S. J.; Ho-Baillie, A. Humidity-Induced Degradation via Grain Boundaries of HC(NH2)(2)PbI3 Planar Perovskite Solar Cells. *Adv Funct Mater* **2018,** *28* (11).
(27) Cordero, F.; Craciun, F.; Trequattrini, F.; Generosi, A.; Paci, B.; Paoletti, A. M.; Pennesi, G. Stability of Cubic FAPbI(3) from X-ray Diffraction, Anelastic, and Dielectric Measurements. *J Phys Chem Lett* **2019,** *10* (10), 2463-2469.
(28) Liu, T. H.; Zong, Y. X.; Zhou, Y. Y.; Yang, M. J.; Li, Z.; Game, O. S.; Zhu, K.; Zhu, R.; Gong, Q. H.; Padture, N. P. High-Performance Formamidinium-Based Perovskite Solar Cells via Microstructure-Mediated delta-to-alpha Phase Transformation. *Chem Mater* **2017,** *29* (7), 3246-3250.
(29) Kim, G. W.; Shinde, D. V.; Park, T. Thickness of the hole transport layer in perovskite solar cells: performance versus reproducibility. *Rsc Adv* **2015,** *5* (120), 99356-99360, DOI: 10.1039/c5ra18648j.
(30) Bu, T. L.; Li, J.; Zheng, F.; Chen, W. J.; Wen, X. M.; Ku, Z. L.; Peng, Y.; Zhong, J.; Cheng, Y. B.; Huang, F. Z. Universal passivation strategy to slot-die printed SnO2 for hysteresis-free efficient flexible perovskite solar module. *Nat Commun* **2018,** *9*, 4609.
(31) Kang, D. H.; Park, N. G. On the Current-Voltage Hysteresis in Perovskite Solar Cells: Dependence on Perovskite Composition and Methods to Remove Hysteresis. *Adv Mater* **2019,** *31* (34), 1805214.
(32) Abdi-Jalebi, M.; Andaji-Garmaroudi, Z.; Cacovich, S.; Stavrakas, C.; Philippe, B.; Richter, J. M.; Alsari, M.; Booker, E. P.; Hutter, E. M.; Pearson, A. J.; Lilliu, S.; Savenije, T. J.; Rensmo, H.; Divitini, G.; Ducati, C.; Friend, R. H.; Stranks, S. D. Maximizing and stabilizing luminescence from halide perovskites with potassium passivation. *Nature* **2018,** *555* (7697), 497–501.
(33) Shao, Y. H.; Xiao, Z. G.; Bi, C.; Yuan, Y. B.; Huang, J. S. Origin and elimination of photocurrent hysteresis by fullerene passivation in CH3NH3PbI3 planar heterojunction solar cells. *Nat Commun* **2014,** *5*, DOI: ARTN 5784

10.1038/ncomms6784.
(34) Xiao, Z.; Dong, Q.; Bi, C.; Shao, Y.; Yuan, Y.; Huang, J. Solvent Annealing of Perovskite-Induced Crystal Growth for Photovoltaic-Device Efficiency Enhancement. *Adv Mater* **2014,** *26* (37), 6503-6509, DOI: 10.1002/adma.201401685.
(35) Deng, Y. H.; Peng, E.; Shao, Y. C.; Xiao, Z. G.; Dong, Q. F.; Huang, J. S. Scalable fabrication of efficient organolead trihalide perovskite solar cells with doctor-bladed active layers. *Energ Environ Sci* **2015,** *8* (5), 1544-1550.
(36) Contreras-Bernal, L.; Ramos-Terrón, S.; Riquelme, A.; Boix, P. P.; Idígoras, J.; Mora-Seró, I.; Anta, J. A. Impedance analysis of perovskite solar cells: a case study. *J Mater Chem A* **2019,** *7* (19), 12191-12200, DOI: 10.1039/C9TA02808K.
(37) Bisquert, J. Interpretation of electron diffusion coefficient in organic and inorganic semiconductors with broad distributions of states. *Phys Chem Chem Phys* **2008,** *10* (22), 3175-3194, DOI: 10.1039/b719943k.
(38) Shao, Y. C.; Yuan, Y. B.; Huang, J. S. Correlation of energy disorder and open-circuit voltage in hybrid perovskite solar cells. *Nat Energy* **2016,** *1*, DOI: Unsp 15001

10.1038/Nenergy.2015.1.
(39) Urbach, F. The Long-Wavelength Edge of Photographic Sensitivity and of the Electronic Absorption of Solids. *Phys Rev* **1953,** *92* (5), 1324-1324, DOI: DOI 10.1103/PhysRev.92.1324.
(40) Nie, W. Y.; Tsai, H. H.; Asadpour, R.; Blancon, J. C.; Neukirch, A. J.; Gupta, G.; Crochet, J. J.; Chhowalla, M.; Tretiak, S.; Alam, M. A.; Wang, H. L.; Mohite, A. D. High-efficiency solution-processed perovskite solar cells with millimeter-scale grains. *Science* **2015,** *347* (6221), 522-525, DOI: 10.1126/science.aaa0472.
(41) Koster, L. J. A.; Mihailetchi, V. D.; Ramaker, R.; Blom, P. W. M. Light intensity dependence of open-circuit

voltage of polymer : fullerene solar cells. *Appl Phys Lett* **2005,** *86* (12).
(42) Green, M. A. Solar-Cell Fill Factors - General Graph and Empirical Expressions. *Solid State Electron* **1981,** *24* (8), 788-789, DOI: Doi 10.1016/0038-1101(81)90062-9.
(43) Guo, X. G.; Zhou, N. J.; Lou, S. J.; Smith, J.; Tice, D. B.; Hennek, J. W.; Ortiz, R. P.; Navarrete, J. T. L.; Li, S. Y.; Strzalka, J.; Chen, L. X.; Chang, R. P. H.; Facchetti, A.; Marks, T. J. Polymer solar cells with enhanced fill factors. *Nat Photonics* **2013,** *7* (10), 825-833, DOI: 10.1038/Nphoton.2013.207.
(44) Li, X.; Huang, J. S.; Nejati, S.; McMillon, L.; Huang, S.; Osuji, C. O.; Hazari, N.; Taylor, A. D. Role of HF in Oxygen Removal from Carbon Nanotubes: Implications for High Performance Carbon Electronics. *Nano Lett* **2014,** *14* (11), 6179-6184, DOI: 10.1021/n1502401c.
(45) Fei, C. B.; Li, B.; Zhang, R.; Fu, H. Y.; Tian, J. J.; Cao, G. Z. Highly Efficient and Stable Perovskite Solar Cells Based on Monolithically Grained CH3NH3PbI3 Film. *Adv Energy Mater* **2017,** *7* (9).
(46) Chu, Z. D.; Yang, M. J.; Schulz, P.; Wu, D.; Ma, X.; Seifert, E.; Sun, L. Y.; Li, X. Q.; Zhu, K.; Lai, K. J. Impact of grain boundaries on efficiency and stability of organic-inorganic trihalide perovskites. *Nat Commun* **2017,** *8*, DOI: ARTN 2230

10.1038/s41467-017-02331-4.
(47) Deng, Y. H.; Zheng, X. P.; Bai, Y.; Wang, Q.; Zhao, J. J.; Huang, J. S. Surfactant-controlled ink drying enables high-speed deposition of perovskite films for efficient photovoltaic modules. *Nat Energy* **2018,** *3* (7), 560-566, DOI: 10.1038/s41560-018-0153-9.
(48) Kim, D. H.; Whitaker, J. B.; Li, Z.; van Hest, M. F. A. M.; Zhu, K. Outlook and Challenges of Perovskite Solar Cells toward Terawatt-Scale Photovoltaic Module Technology. *Joule* **2018,** *2* (8), 1437-1451, DOI: 10.1016/j.joule.2018.05.011.

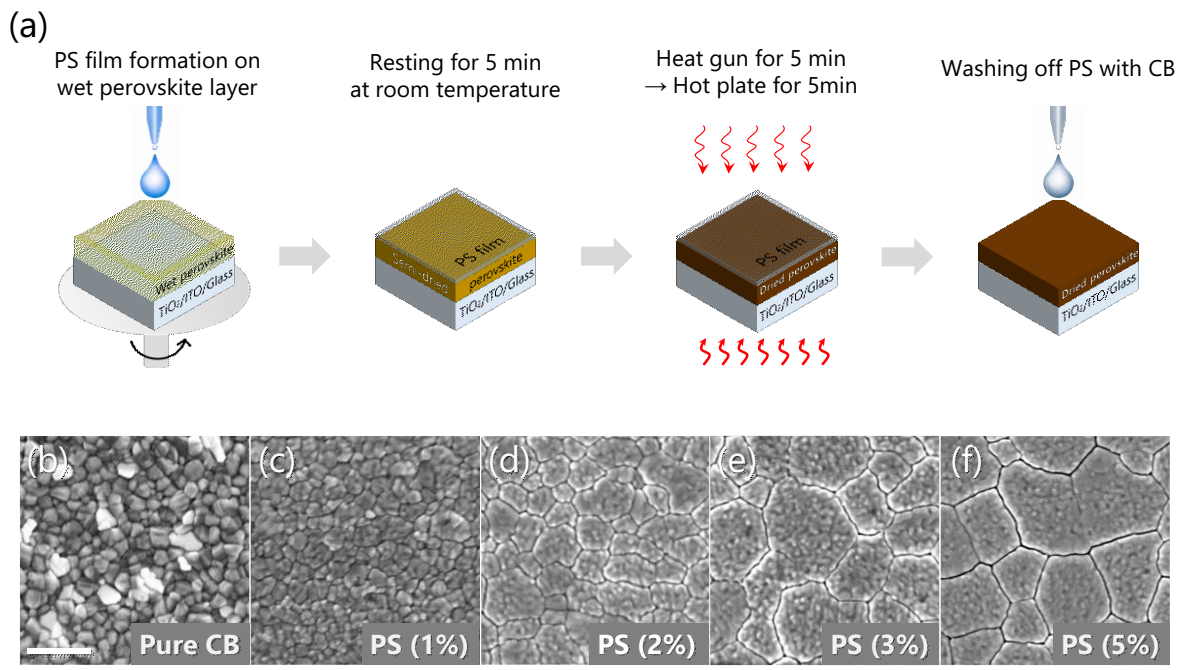

Figure 1. (a) Schematic of the polymer-capped solvent-annealing process during perovskite layer fabrication. Top-down view SEM images of perovskite films fabricated using (b) pure CB, and polystyrene solutions; (c) 1% PS solution, (d) 2% PS solution, (e) 3% PS solution, (f) 5% PS solution, respectively. Prior to the SEM measurements, the PS polymer layers were completely removed by the multiple rinsing with CB solvent. The scale bar is 1 μm.

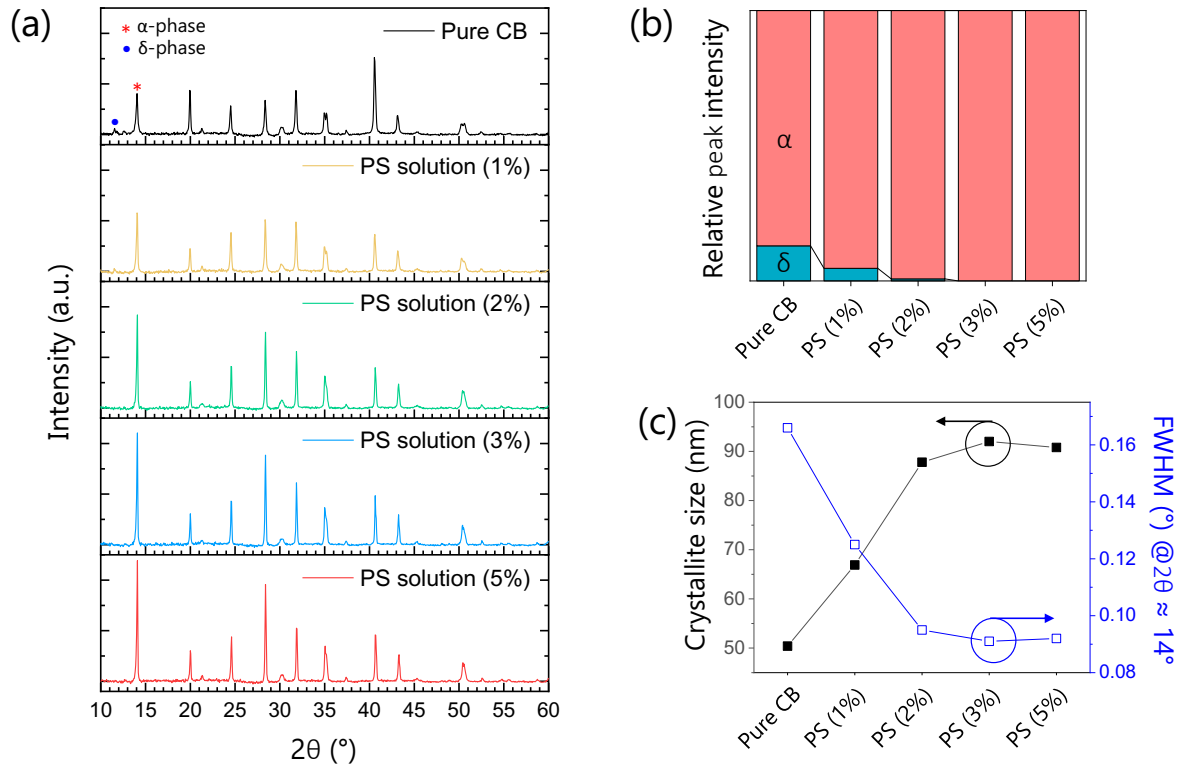

Figure 2. (a) XRD patterns of perovskite films with different concentrations of PS solutions. (b) Relative XRD peak intensities of α-phase and δ-phase crystallites in the perovskite films. The crystallite size was determined from the Scherrer equation. (c) Crystallite size and full width half maximum (FWHM) at $2\theta \approx 14°$ for each sample.

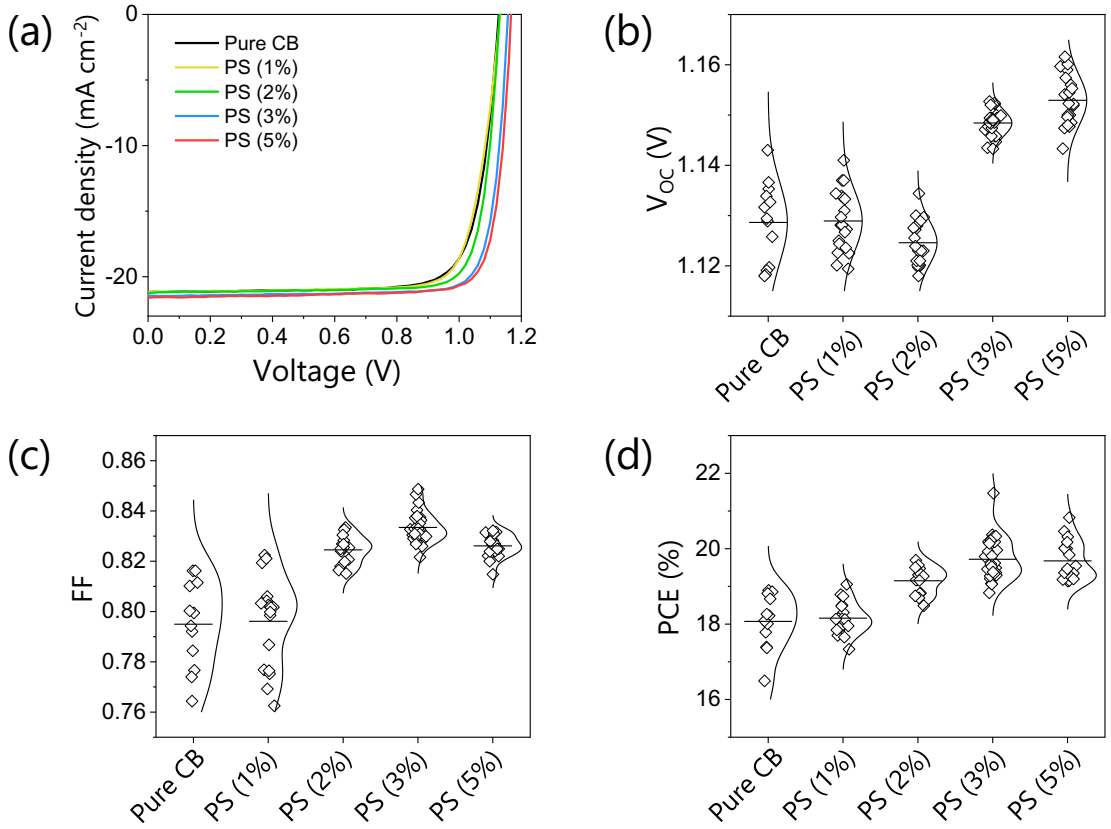

Figure 3. (a) Representative J-V curves, and measured data of (b) V_{OC}, (c) FF and (d) PCE of the perovskite solar cells processed with pure CB and PS solutions with different concentration from 1 to 5%. Kernel smoothing functions were applied to more than 12 data points and were overlaid beside the data points to represent the data statistics.

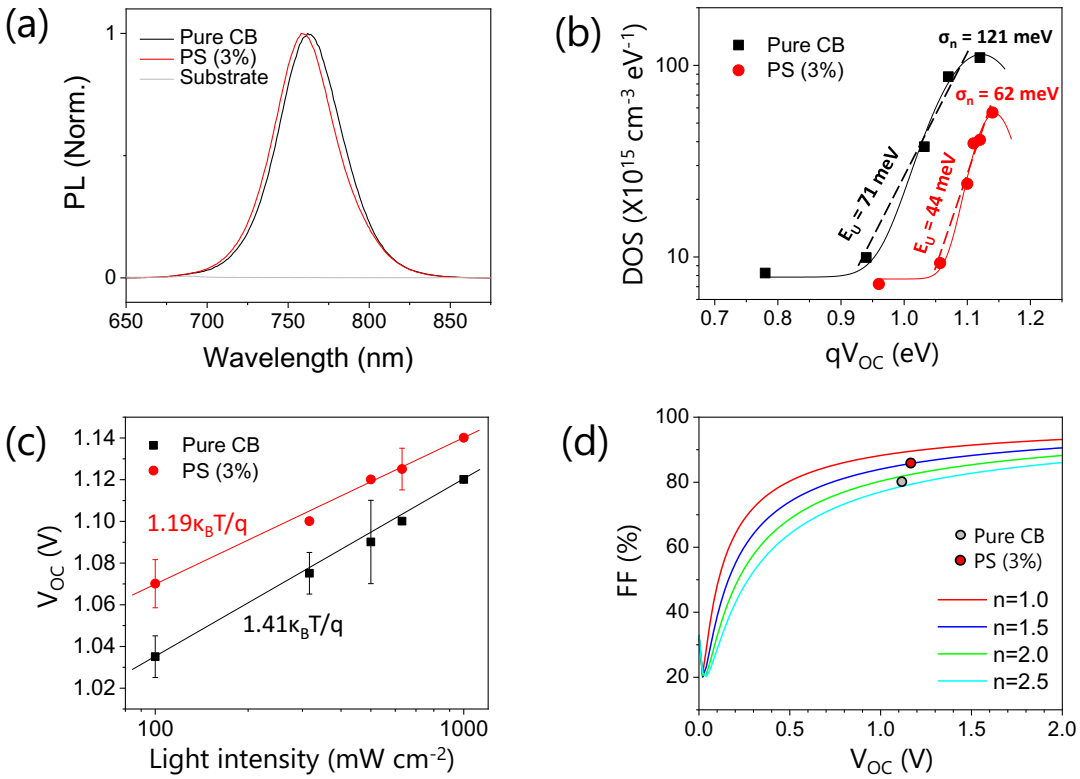

Figure 4. (a) Photoluminescence, (b) DOS of the devices and extracted parameters from a Gaussian or an Urbach tail fitting, (c) light intensity dependence of open-circuit voltage of the solar cells with and without polymer-capped solvent-annealing process, respectively and (d) simulated curves with different ideality factors and the data points obtained from the solar cells with and without polymer-capped solvent annealing, respectively.

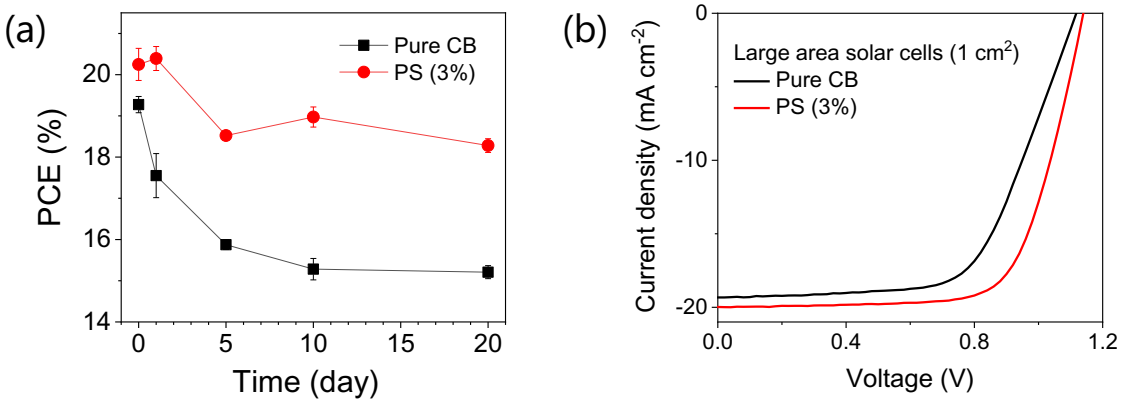

Figure 5. (a) Long-term stability tests of perovskite films in air (RH ≈ 20%, T ≈ 80 °C). (b) *J-V* characteristics of large area solar cells processed with and without polymer-capped solvent annealing, respectively.

TOC graphic

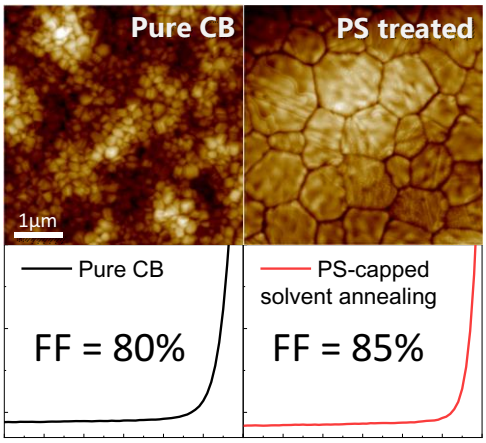
Pure CB
PS treated
1μm
Pure CB
FF = 80%
PS-capped
solvent annealing
FF = 85%